Three-dimensional dendrite-tip morphology

J. C. LaCombe, M. B. Koss, V. E. Fradkov, and M. E. Glicksman
Materials Science and Engineering Department, Rensselaer Polytechnic Institute, Troy, New York 12180-3590
(Received 4 April 1995)

We investigated the morphology of dendrite tips through the growth and measurement of pure succinonitrile dendrites at a fixed supercooling of 0.46 K. Many current theories of dendritic growth rely on the assumption that the tip region can be approximated by a paraboloid of revolution. The evidence presented here suggests that this assumption becomes invalid in regions only slightly removed from the tip and well before the appearance of side branches. Characterization of dendrites using a fourth-order polynomial, with fourfold rotational symmetry, provides a useful description of the dendrite extending to regions up to eight radii from the tip. This has also enabled a more precise determination of the shape and size of a dendrite tip than was heretofore possible. This includes information about the anisotropy of the interface morphology.

PACS number(s): 68.70.+w, 68.35.Bs, 81.30.Fb, 61.50.Cj

I. INTRODUCTION AND BACKGROUND

Solidification processes in many common engineering materials frequently produce morphologically complex dendritic microstructures. The study of the formation of dendrites is important because the initial, or "as cast," microstructure dictates many of the resulting material properties. If a better understanding of the physical processes by which dendrites form can be achieved, both improved theories and manufacturing processes can subsequently be developed.

Dendritic microstructures are commonly observed in processes where the driving forces (thermal and/or solutal gradients) are relatively small and where the materials exhibit relatively little crystalline anisotropy. These conditions are common to many solidification processes, ranging from the casting of metals and alloys to welding. A review of the salient physics of dendritic growth as well as a summary of current theories can be found in a recent review by one of the authors [1].

To date, the principal theoretical developments concerning dendritic growth include the assumptions that a dendrite tip can, to a good approximation, be represented by a paraboloidal body of revolution growing at a constant velocity. Given these assumptions, Ivantsov has shown the solution of the pertinent steady-state heat transport equations to be [2]

$$\mathrm{St}=\mathrm{Pe}\left[e^{\mathrm{Pe}}\int_{\mathrm{Pe}}^{\infty}\frac{e^{-u}}{u}du\right], \tag{1}$$

where $\mathrm{St}\equiv\Delta T/(L/C_p)$ defines the Stefan number (the dimensionless supercooling), $\mathrm{Pe}\equiv VR/2\alpha$ defines the growth Péclet number, ΔT is the supercooling, L is the molar latent heat, and C_p is the molar specific heat under constant pressure. V represents the steady-state dendrite-tip velocity, α is the thermal diffusivity of the liquid phase, and R is a length scale, taken here to be the radius of curvature at the paraboloidal dendrite tip.

If the Ivantsov equation, Eq. (1), is written as $\mathrm{St}=I_v(\mathrm{Pe})$, where the function, $I_v(\mathrm{Pe})$ represents the right-hand side of Eq. (1), then the product VR can be obtained as a function of the independent variable ΔT from the inverse relation $\mathrm{Pe}=I_v^{-1}(\mathrm{St})$. Upon rearranging, and formally inverting this formulation, we obtain

$$VR=2\alpha I_v^{-1}(\mathrm{St})\ . \tag{2}$$

Equation (2) does not uniquely specify the operating state of this system. In order to determine V and R separately as functions of the supercooling (St, or ΔT), a second relationship, independent of Ivantsov's theory, is needed. This relationship, first suggested from Oldfield's considerations of the stability of the growth interface [1], is

$$VR^2=\mathrm{const}\ . \tag{3}$$

Combining Eqs. (2) and (3) makes it possible to predict the dendritic growth rate V as well as a morphological length scale parameter R as independent functions of the supercooling. Exploration of the validity of the tip shape approximation as a paraboloidal body of revolution is the primary focus of this work.

The results of this study show that the shape of the tip region of a dendrite cannot be represented accurately by a paraboloid of revolution. However, when a second parameter, in addition to R, is included in the characterization, the tip region can be represented sufficiently accurately through the use of a fourth-order polynomial with fourfold rotational symmetry incorporated into the fourth-order constant.

It has long been recognized that dendrites are not paraboloids of revolution—particularly if one considers the regions slightly displaced from the tip. This is illustrated in Fig. 1 [3] where two succinonitrile dendrite images are superimposed upon one another. Here, one tip ($\phi=0°$) viewed along a ⟨100⟩ direction appears wider than a "best-fit" parabola (dotted line), and a second image ($\phi=45°$) obtained from the ⟨110⟩ direction is seen to be narrower than the "best-fit" parabola. One should note, however, that close to the tip, the two views do in fact

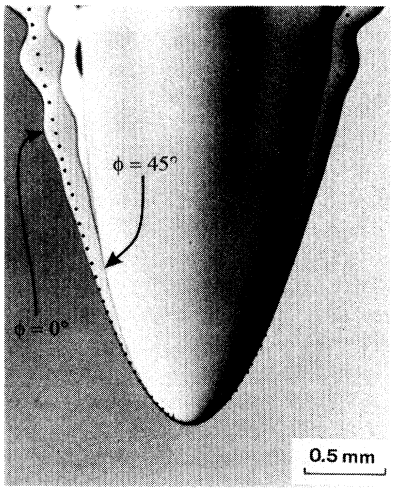

FIG. 1. SCN dendrite tip viewed from two orientations. This illustrates [3] the difference in shape of two superimposed views of the same dendrite. The view from $\phi = 0°$ was made by imaging a dendrite from the direction of the side branches, while $\phi = 45°$ represents a view from between the side branches. A best-fit parabola is indicated by the dotted line between these two profiles.

start to approximate more closely the "best-fit" parabola. This observation justifies the basis of why most efforts in measuring R, to date, have made use of a parabolic (second-order polynomial) fitting form (see, for example, Refs. [3–6]).

A fundamental difficulty in quantifying dendritic tip shapes is that in order to obtain the radius of curvature *at* the tip, it is necessary to use information that comes from regions of the solid-liquid interface *away* from the tip. It has been observed by several investigators [4,7] that the quality of shape information captured in optical images obtained near the tip is not as high as that taken from regions further away. The tip, in addition to being the region of the highest geometric curvature, is also the region of the interface surrounded by the steepest gradients, where the distortion due to variations in the melt's refractive index is greatest. A second detrimental effect is the influence of the "optical point spread function" at the tip. This effect, resulting from the spreading of a theoretical point source due to aberrations in the optics system [8] becomes more important at the tip, where these point spread functions begin to overlap. These issues make it difficult to locate accurately the crystal/melt interface of the dendrite near the tip. Furthermore, regression techniques employed for computing the tip curvature typically rely more on the information taken from the tip of the dendrite. This last issue can, however, be dealt with through the use of somewhat more elaborate weighting schemes in the regression calculations which favor the data farther from the tip, where the deviations from parabolicity become more evident.

A paraboloidal dendrite tip will display a two-dimensional (2D) projection (or shadow profile) of its solid-liquid interface that can be represented with a second-order polynomial equation in Cartesian coordinates. This shape takes the functional form for a vertically opening parabola of

$$y = y_0 + \frac{1}{2R}(x - x_0)^2 , \tag{4}$$

where x and y are the coordinate directions, R is the radius of curvature at the tip, and the point (x_0, y_0) represents the location of the tip. In this form, Eq. (4) is nonlinear in the fitting parameter x_0. If the following substitutions are made,

$$a_0 = \frac{x_0^2}{2R} + y_0, \quad a_1 = \frac{-y_0}{R}, \quad a_2 = \frac{1}{2R} ,$$

it is then possible to rewrite Eq. (4) as a standard second-order polynomial,

$$y = a_0 + a_1 x + a_2 x^2 . \tag{5}$$

In this form, profile data from micrographs of growing dendrites can be fitted using standard linear regression techniques to produce values for a_0, a_1, and a_2, from which x_0, y_0, and R can be calculated.

The curvature of any 2D, single-valued function $y = f(x)$ is given by the standard differential expression

$$\kappa = \frac{|f''(x)|}{[1 + f'(x)^2]^{3/2}} , \tag{6}$$

where $f'(x)$ and $f''(x)$ represent the first and second derivatives, respectively. When Eq. (6) is applied to the second-order polynomial, Eq. (5), it yields the radius of curvature (R) at the tip ($x = x_0$) of

$$R = \frac{1}{\kappa} = \frac{1}{2a_2} . \tag{7}$$

The combination of the second-order polynomial, Eq. (5), with the tip curvature, Eq. (7), yields the shape relationship for the tip region given initially in Eq. (4).

Several other methods appear in the literature to extract radii measurements from crystal/melt edge profiles. For example, if one locates the tip of the parabola at the origin of the coordinate system, then Eq. (4) reduces to

$$y = \frac{1}{2R} x^2 . \tag{8}$$

This relationship is represented in Fig. 2, where $w = 2x$, and $L = y$. Substituting these definitions into Eq. (8) yields the parabola

$$w^2 = R\,8L . \tag{9}$$

Equation (9) indicates that if w^2 is plotted against $8L$, the resulting slope would be the radius of curvature at the tip of the parabola R. If one uses this approach with an experimental data set from a dendrite tip profile, the slope will not remain constant for all L, *unless the tip shape is exactly paraboloidal.*

Use of this procedure requires that the dendrite tip be vertically oriented, and that the tip be located at the origin. The location of the tip may be identified using several techniques, including calculation of the average x

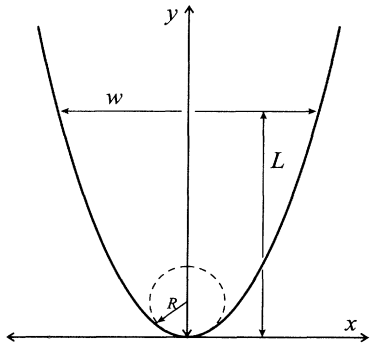

FIG. 2. Parabola with tip located at origin. The radius of curvature at the tip is identified as well as the width (w) at position $y=L$.

value in the data set, locating the lowest y value in the data set, or by "eyeball" approximation.

A more robust procedure would allow the tip of the dendrite to be located at positions other than the origin. Combining the second-order polynomial, Eq. (5), with a linear regression technique, x_0, y_0, and R can all be determined given a set of x-y coordinates representing the tip profile. If the tip location is identified via regression, rather than by less reliable approximations such as those described above, then the error incurred near the tip region where the model is particularly sensitive is minimized. *All* of these radii calculations, however, are limited by the stringent assumption of a parabolic tip profile.

Several researchers have suggested that a higher-order polynomial model be used to characterize the shape of dendrite tips [6,9–12]. The parabolic profiles described previously quickly become inaccurate away from the tip, often well before side branching becomes dominant. Maurer, Perrin, and Tabeling's suggested improvement [6] adds a shape modulation based on $\cos(4\phi)$, reflecting the fourfold symmetry of many cubic dendritic crystals. The suggested tip profile may be expressed as

$$Y=\frac{X^2}{2}[1+\alpha\cos(4\phi)]-\delta X^4\cos(4\phi)\ , \tag{10}$$

where $Y=y/R$, $X=x/R$, and α and δ are fitting coefficients. Maurer, Perrin, and Tabeling [6] have found the coefficient α in NH_4Br dendrites to be negligible, resulting in the fourfold symmetry being restricted to the fourth-order term, namely,

$$Y=\frac{X^2}{2}-\delta X^4\cos(4\phi)\ . \tag{11}$$

Theoretical models developed by Kessler and Levine, Ben-Amar and Brener, and Brener [9–12] have recently been proposed for describing the steady-state three-dimensional shape of dendrites when anisotropy of the interfacial energy is incorporated [11]. The typical anisotropic shape, one form of which is given by Brener, incorporates a term for each of the azimuthal modes [12],

$$Y=-\frac{X^2}{2}+\sum A_m X^m\cos(m\phi)\ . \tag{12}$$

For a crystal with fourfold cubic symmetry, the first non-negligible correction term to the parabola is the fourth-order harmonic ($m=4$). If Eq. (12) is limited just to this $m=4$ term, it can be reduced to the form of Eq. (11), excepting the sign convention.

II. EXPERIMENT DESCRIPTION

The experiments conducted in this investigation were performed using ultrapure succinonitrile [SCN, chemical formula: $CH\text{-}(CH_2)_2\text{-}CN$] in a temperature-controlled environment with a stability of ± 1 mK. 32 dendrites were grown with an average observed supercooling of $\Delta T=0.461\pm0.002$ K. Figure 3 shows a schematic diagram of the experimental setup. In an effort to obtain optimum optical quality for the images, the heat transfer medium used in the thermostated bath surrounding the growth chamber is a transparent mixture of water and ethylene glycol of a composition ($\sim 87\%$ ethylene glycol) that matches the index of refraction of the molten SCN. The growth chamber containing the purified SCN (99.999% pure) was designed as part of the isothermal dendritic growth experiment [5] and is constructed solely of stainless steel and borosilicate glass for ruggedness, and to minimize the chemical interaction between the SCN sample material and the container. These materials were selected following extensive chemical compatibility studies by Rubenstein, Tirmizi, and Glicksman [13] and have proved not to degrade the purity of the SCN stored in such chambers over periods of time exceeding three years.

The process of growing a dendrite starts by melting the SCN and then lowering the bath temperature to the desired supercooling, while maintaining the SCN within the growth chamber in the liquid state. Once thermistors located within the chamber (Fig. 4) indicate thermal stabilization at the predetermined supercooling level, a thermoelectric cooler is activated to cool the end of a tube filled with a small amount of SCN (the "stinger" in Fig. 4). The molten SCN within this tube starts to solidify, and the solidification front propagates along the tube until it emerges into the large volume of liquid SCN in the main chamber. Once free of the confinement of the stinger tube, a dendrite proceeds to grow freely into the

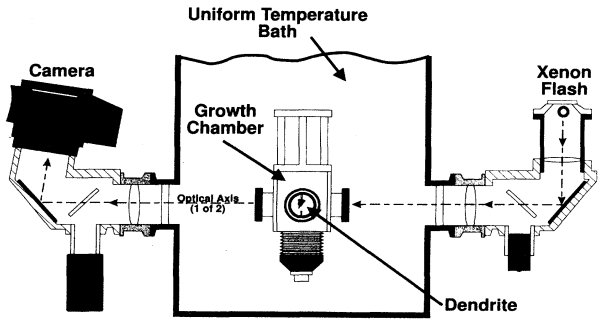

FIG. 3. Schematic representation of the experiment. A growth chamber with four perpendicularly oriented windows is placed in a uniform temperature bath. After nucleation, dendrites are photographed at regular time intervals along two perpendicular directions.

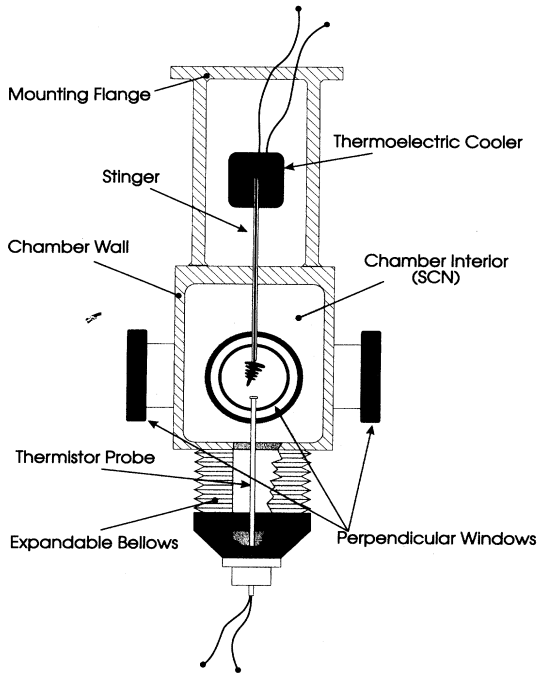

FIG. 4. Schematic representation of growth chamber. The thermoelectric cooler induces nucleation that propagates along the stinger tube and into the chamber interior where a single crystal dendrite is free to grow.

melt, forming a three-dimensional dendritic equiaxed crystal. At this point, 35-mm photographs are taken at regular time intervals along the two perpendicular optical paths. Typical photographs, as seen in Fig. 5, serve as the primary source of dendrite tip-shape information used in these experiments.

The 35-mm negatives are analyzed using a combination of microscope/vernier measurements and computer-based image processing. The vernier stage is used with a microscope to locate the position of the dendrite tip as it changes over time in each of the orthogonal views. This yields the tip position as a function of x,y,z and time. The tip velocity vector is calculated from these data and provides an indication of steady-state growth as well as the Eulerian angles of the growth velocity vector with respect to a coordinate system aligned with the stinger tube axis. Next, using a PC-based image-capture system,

FIG. 5. 35-mm film image of SCN dendrite growing isothermally at $\Delta T=0.46$ K. Photos are taken along perpendicular axes to produce velocity, size, and shape information.

the dendrite tip images are digitized. The digitized images are analyzed, producing a set of ordered pairs (x,y) of the solid-liquid interface positions for each dendrite. There are several methods available for locating the interface (the optical dendrite edge), and are discussed in more detail by Dougherty and Gollub in Ref. [4] and by Glicksman *et al.* in Ref. [7].

Once the edge has been located and reduced to the form of a set of x-y coordinate pairs, these data can then be analyzed using a variety of methods to determine the length scale of the dendrite tip. The primary focus of this work is delineating the process of determining the three-dimensional size and shape of dendrites.

III. FOURTH-ORDER POLYNOMIAL CHARACTERIZATION METHOD

It is proposed here that a fourth-order polynomial provides an improved description of the three-dimensional shape of a dendrite tip in comparison with standard results obtained using second-order parabolic models. The equation used in this study is a simple extension of the second-order polynomial, Eq. (4), namely

$$y=y_0+\frac{1}{2R}(x-x_0)^2+q(x-x_0)^4 , \tag{13}$$

where q has units of length^{-3} and represents the amplitude of the quartic deviation from parabolicity. Later, we will incorporate rotational asymmetry of the shape, arising from anisotropy effects, through this fourth-order coefficient. This avoids the need to assume the anisotropy function *ab initio*. Notice that Eq. (13) is again nonlinear in the fitting parameter x_0, but this time, cannot be rewritten in a form that can be fitted using a linear regression technique as was done when the second-order shape described by Eq. (4) was transformed into the standard polynomial form of Eq. (5). Attempts at transforming the fourth-order shape equation, Eq. (13), into a simpler form result in an overspecified system. Five equations result, but they are not linearly independent, because there are only four independent parameters (x_0, y_0, R, and q). In order to fit dendrite edge data to this relationship, standard nonlinear regression techniques may be applied to the fourth-order shape equation, Eq. (13). However, a more efficient scheme has been developed as part of this work.

The relationship in Eq. (13) is fit here by fixing the parameter x_0 and performing a standard *linear* regression such as a fourth-order polynomial fit with the first- and third-order coefficients set to zero. If we let $x'=x-x_0$, then the equation can be written as

$$y=y_0+\frac{1}{2R}(x')^2+q(x')^4 . \tag{14}$$

With the resulting fitted coefficients, a value for the "goodness of fit" is determined using the expression

$$\chi^2=\frac{\sum(y_{\text{exp}}-y_{\text{fit}})^2}{n-4} , \tag{15}$$

where y_{exp} and y_{fit} represent the experimental and fitted

data points, respectively, and n is the number of data points used in the regression. The fitting process is repeated systematically by choosing new values of x_0 and recalculating the other fitting constants and the corresponding χ^2. The value of x_0 that produces fitting constants which result in the minimum χ^2 is taken to be the "best fit." When performed iteratively, using a computer, the selection of x_0 for minimization of χ^2 is done using a secant method.

Application of the curvature equation, Eq. (6), to the higher-order tip shape in Eq. (13) indicates that the radius of curvature at the tip of the dendrite remains a function of only the second-order term. This allows the axisymmetric, paraboloidal contribution of the shape to be exclusively determined by the second-order coefficients, leaving the higher-order terms to describe the asymmetric deviations occurring away from the tip. Thus, adding higher-order terms to the parabolic model reduces the orientation dependence of the measured radius.

IV. RESULTS AND DISCUSSION

Several researchers [3,4,6,14] have already shown in their results that the paraboloidal shape assumption of the dendrite tip does not hold away from the tip. By varying the data range (starting from the tip) used in the regression analysis of the second-order polynomial, Eq. (5), the measured radius is observed to vary approximately linearly with the range of data. Results from this type of analysis are shown in Fig. 6 for dendrites from our experiments viewed from three different directions.

Figure 6 contains several points of interest. If the assumption of a paraboloidal shape is valid, then as shown by Eq. (7), the fitted radius of curvature should not depend on the data range used in the regression; i.e., R should be a constant. Inspection of this figure shows that as the sampling region is increased, the radius is *not* generally constant. Instead, as shown for two of the three dendrites viewed from different orientations, the observed radii of curvature deviate steadily from the paraboloidal radius of curvature. However, when a dendrite is observed from an orientation of approximately $\phi \approx 30°$, the profile is close to a parabola. Evidence of this is seen in the third dendrite represented in Fig. 6, where a nearly constant value of R is observed as the sampling region is extended away from the tip. A second point of interest in this figure is noted by extrapolating the data back to the point where the sample range $y_{max}=0$. Here, a value of the radius of curvature *at the tip* may be deduced by extrapolation. This extrapolation is used to represent what the radius would be, were it possible to measure the curvature directly (and reliably) at the tip. Inspecting the data from each of the different view directions shows that this extrapolated tip radius varies less with the view direction than do radii measurements taken at any other value of the ordinate. Using this technique, any of the three data sets in this figure can be extrapolated back to the tip where the individual tip radii approach a common value.

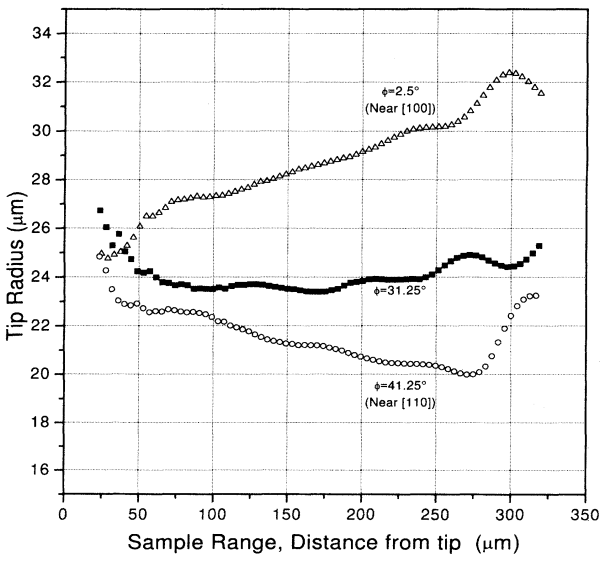

FIG. 6. Radius as a function of sampling range for a second-order polynomial regression model based on Eq. (5). The radius at the tip can be obtained by extrapolating the plot to $y_{max}=0$. Data are shown for dendrites observed from three different directions: $\phi=41.25°$, $31.25°$, and $2.5°$.

These results *clearly* illustrate that dendrites are not bodies of revolution. In addition, commonly observed fourfold rotational symmetry that is associated with the side branch planes in cubic materials cannot be characterized using a second-order polynomial model. The extrapolation methods, however, described above (and in Fig. 6), can improve the results. It now becomes clear that the paraboloidal model should be modified to permit more precise description of a dendrite tip.

As discussed earlier, the experimental data that were obtained in this study consist primarily of x-y coordinates of dendrite-tip profiles observed from varying projection orientations ϕ. By fitting these data to the fourth-order shape of Eq. (13), relationships between R and q and the view direction ϕ can be obtained. The fourth-order coefficient can be scaled conveniently as $Q=qR^3$ to account for minor fluctuations in the supercooling and any convective influences reflected in R. Since the parameters x_0 and y_0 in Eq. (13) do not describe the tip shape, the basis shape can also be scaled by the tip radius to produce a nondimensional form similar to Eq. (11), namely,

$$Y=\frac{X^2}{2}+Q(\phi)X^4 , \tag{16}$$

where $Q(\phi)$ is free to vary as a function of the projection direction ϕ.

Figure 7 shows that the application of a fourth-order polynomial to the regression of the tip profile data provides better qualitative and quantitative agreement than does the second-order polynomial to a region extending much further from the tip. We note that the two models agree well near the tip. The second-order fit, however (no matter how R is extracted from the tip profile data), starts to deviate noticeably from the profile at approximately three to four radii from the tip. The fourth-order fit, by contrast, continues to agree well with the tip

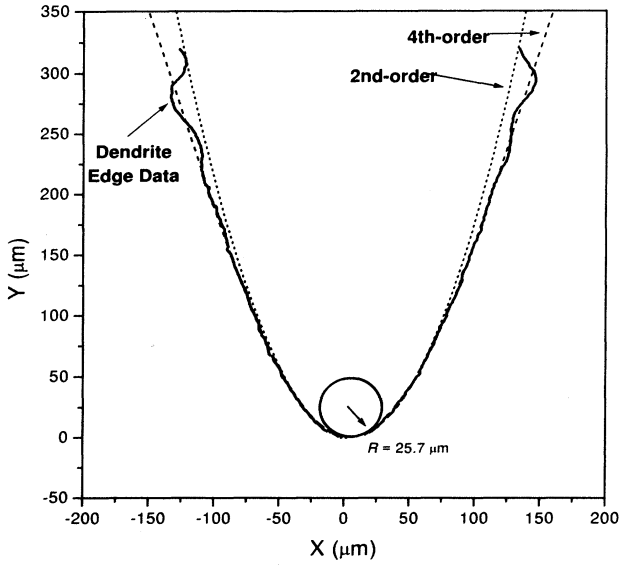

FIG. 7. Second- and fourth-order polynomial fits superimposed upon the edge data. The fourth order fit is seen to be qualitatively better away from the tip region. Near the tip region, however, the two models agree well.

profile to beyond eight radii, which is a region sufficiently remote from the tip where side branches become visible. Improvement in the radii data is also evident in Fig. 8, which shows that when using a fourth-order fit, the direction from which the measurement is made is much less influential than for the case of the second-order fit (compare with Fig. 6). Since regions of the interface displaced further from the tip have an increasing presence of side branches, the tip radius should be obtained by taking an average over the sample ranges of the tip exhibiting relatively constant value, where the influence of side branches is not significant. Figures 7 and 8 illustrate that this plateau is typically beyond the region proximate to the tip (where scatter in the data is more influential), but not so far from the tip that side branches are present. This process of selecting the region over which to take the average is consistent with numerical calculations we performed using an exact fourth-order function with 1-μm Gaussian scatter added to the profile data. The selection of the region over which to calculate the average does involve judgment, but in comparison to making similar measurements using the second-order methods discussed previously, this technique is less subjective and appears to produce more reliable tip radii data with less scatter.

If the tip region of a dendrite can be characterized quantitatively in the mathematical form of Eq. (13), then a dendrite observed from *any* direction should produce the same fitted value for the radius. Potentially, such a procedure would be useful for making experimental measurements of tip radii, as it would no longer be necessary to make measurements from a particular direction.

Figure 9 shows the measured tip radii as a function of the projection orientation from which the dendrite profile was observed. Of the 32 dendrites grown, 22 images were usable for shape measurements, due primarily to restrictions on image quality. Inspection of these data shows that the spread in the radii is ± 1.5 μm over most of the range of ϕ. This is approximately a 50% reduction in spread compared with tip radii data obtained using parabolic regression techniques. It is not clear whether the slight downward trend in radii (as ϕ is increased) is real, because this variation in R is comparable to the size of the uncertainty in the radii data. Furthermore, the data becomes somewhat sparse as ϕ exceeds about 25°.

The dimensionless form of the fourth-order constant (Q) is plotted as a function of observation angle ϕ in

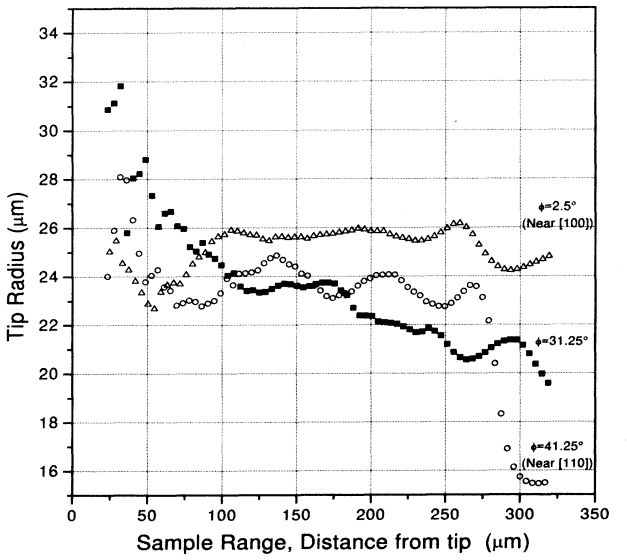

FIG. 8. Radius as a function of sampling range for a fourth-order polynomial regression model based on Eq. (13). Less sensitivity is seen over the sampling range, particularly in the region closer to the tip where side branches are not prevalent (for example, side arms appeared at about 175 μm for the case of $\phi = 31.25°$).

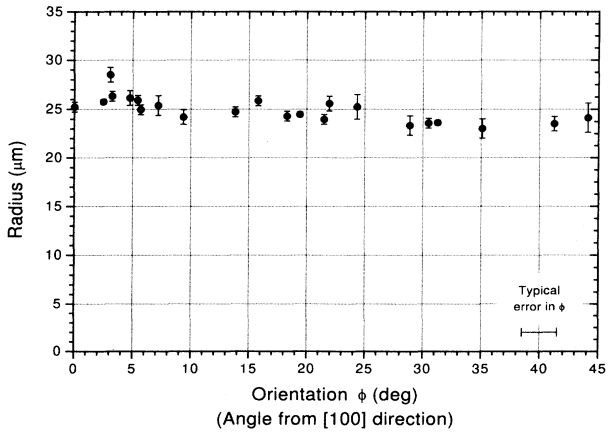

FIG. 9. Dendrite-tip radius as a function of orientation calculated using fourth-order polynomial regression. 22 of the 32 dendrites grown at 0.46 K produced usable tip shape data.

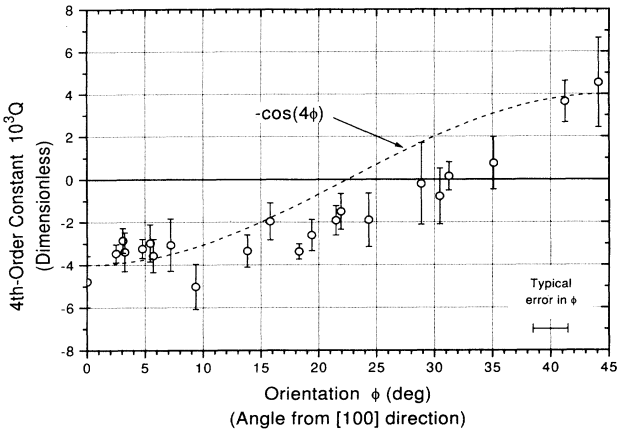

FIG. 10. Fourth-order constant Q as a function of orientation. Q drops to zero, resulting in a parabolic profile, at $\phi \approx 30°$, rather than $\phi \approx 0°$ (commonly believed), or $\phi \approx 22.5°$ [as suggested by Eqs. (11) and (12)].

Fig. 10. A pronounced variation in Q is noted as the dendrite is viewed from different azimuthal directions. The profile of a dendrite will become a parabola when observed from the orientation ϕ, for which Q is zero. The figure indicates that this occurs when $\phi \approx 30°$ rather than $\phi \approx 0°$ (note, $\phi \approx 0°$ is the [100] direction), which was assumed to be the principal projection direction closest to a parabolic profile [3]. The projection angle, $\phi \approx 30°$, also differs from the value of $\phi \approx 22.5°$ that is consistent with the $\cos(4\phi)$ anisotropy terms in Eqs. (11) and (12). The amplitude of the variation in Q is approximately $A \approx 0.008$ over the azimuthal angle range of 0°–45°. Closer inspection of the figure also reveals that the midpoint of this variation does not occur at $\phi = 22.5°$, which would be expected if Q were of the form $Q = f(\cos(4\phi))$. Instead, it occurs at $\phi \approx 30°$, somewhat shifted to the right. If we examine only the amplitude of Q, the experimentally observed value of the ratio $A/2 \approx 0.004$ can be compared to Brener's theoretically predicted value for SCN [12] of $A_4 = 1/88 = 0.011$ resulting from Eq. (12). Note that in order to determine the variations of Q and R with ϕ, it is required that ϕ be determined. The procedure for making this measurement when using fixed camera positions (as described earlier) is discussed in the Appendix.

These observations imply that the use of Eq. (11) may not characterize the tip region accurately. Equation (12), with terms for $m = 4, 8, \ldots$ may be required. However, even without this analysis, we can draw a smoothed curve to describe the measured variation of Q with ϕ shown in Fig. 10. Combining this representation of Q, with an average value of R from Fig. 9, we have fully parametrized the dendrite in accordance with the fourth-order equation as described in Eq. (14). We then used this equation to form a contoured plot of an average three-dimensional dendrite tip, projected along the ⟨100⟩ growth direction, at a supercooling of 0.461 K (Fig. 11). This contour mapping, with contours at $1R$ increments of the y coordinate, fits the R and Q data from the experiments described herein. It exhibits in a compact graphical form many of the key features of a *true* three-dimensional dendrite tip, in the region close to the tip, before the appearance of side branching. This plot should not be confused with similar contour plots, based on qualitative analysis, that are used for illustrative purposes only.

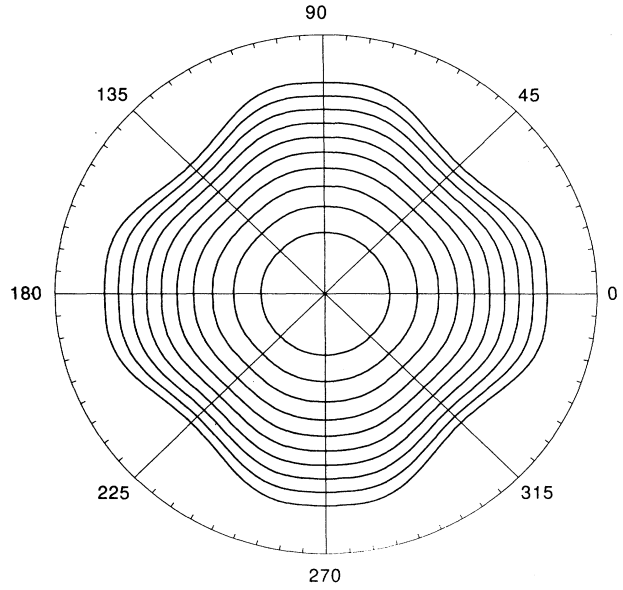

FIG. 11. Contour plot of an "average" dendrite resulting from experimental measurements of the tip region, before the appearance of side branches. Contours are drawn at intervals of $1R$ along the dendrite axis, starting from the tip.

V. CONCLUSIONS

The method for characterizing dendrite-tip shapes presented herein demonstrates that a paraboloid of revolution does not accurately describe the shape of a dendrite tip.

These data provide an experimental description of the three-dimensional shape of dendrite tips that can be employed as a test for theory. These data can also be used for comparisons with dendrite-tip shapes resulting from three-dimensional phase field models such as those performed by Kobayashi in Ref. [15].

The use of a fourth-order polynomial provides, in addition, a 50% reduction in the uncertainty levels of measured tip radii data. It is not conclusive, however, whether or not this process entirely removes the orientation dependence of the tip radii values.

It has been shown that dendrite tip shapes differ somewhat from previous assumptions. Tips viewed from the [100] direction are not parabolic in profile, and a $\cos(4\phi)$ shape modulation does not seem to describe the observed azimuthal form of the nonaxisymmetric variation in cross section caused by crystalline anisotropy.

VI. SUMMARY AND ONGOING ACTIVITIES

By using a fourth-order polynomial to describe the three-dimensional shape of a dendrite tip, the dendrite

morphology can be characterized accurately up to the region where side branches are present.

The azimuthal variation of the asymptotic portion of the tip shape does not follow the $\cos(4\phi)$ form suggested for cubic crystals. It may be necessary to include higher mode terms ($m=8$, etc.) in the regression analysis using a relationship such as Brener's Eq. (12) [12].

The work presented here has introduced several issues that could be explored further from both experimental and theoretical perspectives. Current efforts involve improving experimental and data processing procedures. Experiments similar to those described here are underway, investigating the dendritic tip shape at various supercoolings. In addition to this, experiments are being considered that will permit three-dimensional morphology measurements on a *single* dendrite, rather than a large set of dendrites. This will dramatically speed up the experimental process and minimize the effects due to natural variation among dendrites.

A set of experiments are currently scheduled to be conducted by NASA in low Earth-orbit microgravity conditions aboard the USMP-3 space shuttle platform in early 1996. These experiments are specifically aimed at determining the effect that buoyancy convection has on the three-dimensional shape of SCN dendrites.

ACKNOWLEDGMENTS

This work was generously supported under NASA Contract No. NASA-25368 and the NASA Graduate Student Researcher Program. The authors wish to thank E. A. Winsa at NASA's Lewis Research Center for the use of their experimental facilities, data, and expert advice, as well as L. T. Bushnell, P. Kobryn, and J. L. Oudemool for assistance in analyzing data and for many fruitful discussions.

APPENDIX

Given a pair of images of a dendrite, obtained from two perpendicular directions, it is possible to discern the orientation of the dendrite from which the images were obtained. The angle of this direction (depicted in Fig. 12) is referred to here as the *projection orientation* (ϕ). This figure shows a schematic diagram of the dendrite cruciform with some of the key features identified. The projections (indicated in figure) represent the view seen in the pair of orthogonal images

The orientation ϕ is identified as being the angle between the view plane and any side branch plane. Due to the fourfold rotational symmetry, it does not matter which of the 4 side branch planes is used. We denote the following vectors as indicated in Fig. 12: $\vec{P}$ denotes primary arm vector (unit vector in the direction of the primary dendrite). $\vec{S}$ denotes side arm vector (unit vector in the direction of side branch or alternate primary dendrite). $\vec{V}$ denotes view vector (unit vector in the view direction: can be taken along the coordinate axis such as Z).

These three vectors can be combined to define two planes: Side branch plane: vectors $\vec{S}$ and $\vec{P}$; view plane: vectors $\vec{V}$ and $\vec{P}$. These two planes intersect along the primary dendrite arm (vector $\vec{P}$). The angle between these two planes is determined from the angle between their normals, determined using the cross product of any two vectors in each respective plane:

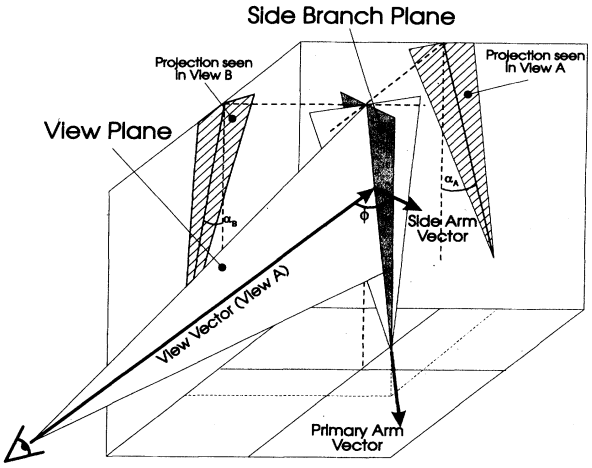

FIG. 12. Schematic representation of dendrite with the projections that would be seen when viewed from two orthogonal directions.

$$\text{Side branch plane normal: } \vec{N}_S=\vec{P}\times\vec{S}\ , \tag{A1a}$$

$$\text{View plane normal: } \vec{N}_V=\vec{P}\times\vec{V}\ . \tag{A1b}$$

The orientation (the angle between these two planes) is thus determined using the vector dot product:

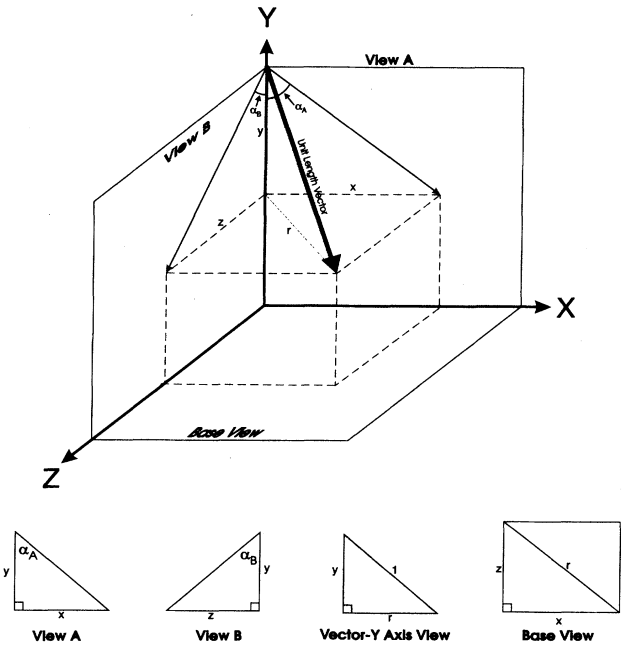

FIG. 13. Identification of vectors representing an arbitrary dendrite arm (primary or secondary).

$$\cos\phi=\frac{\vec{N}_S\cdot\vec{N}_V}{|\vec{N}_S||\vec{N}_V|}=\hat{\vec{N}}_S\cdot\hat{\vec{N}}_V$$

(if $\hat{\vec{N}}_S$ and $\hat{\vec{N}}_V$ are unit vectors) . (A2)

This can be further reduced to a value between 0° and 45°. Doing so will produce a ϕ value that will represent the angle between the view direction and the nearest side arm plane. This is done using

$$\phi=45°-|(\phi \bmod 90°)-45°| \ . \quad \text{(A3)}$$

If the dendrite is a cubic crystal structure with side arms growing in the ⟨100⟩ directions, ϕ will range from 0° along ⟨100⟩ directions to 45° in the ⟨110⟩ directions. This choice is arbitrary and made only for convenience.

In order to make use of this technique, it is necessary to have vector information of the primary dendrite arm and a secondary arm (both assumed to grow along ⟨100⟩ directions). Such information can be derived by measuring the projected angle of these arms as seen in each of the two orthogonal images. Note that it is important that the *same* arm is measured in each of the two perpendicular views. Figure 5 shows a typical image from which the measurements are made.

Figure 13 depicts a unit vector representing the dendrite arm being considered (either the primary or a secondary arm). The only measured parameters needed are the projected angles from each view: α_A and α_B. After performing some trigonometry, the following components of the unit vector are found:

$$x=+\left[\frac{1}{1+\tan^2(\alpha_A)+\tan^2(\alpha_B)}\right]^{1/2}[\tan(\alpha_A)] \ , \quad \text{(A4a)}$$

$$y=-\left[\frac{1}{1+\tan^2(\alpha_A)+\tan^2(\alpha_B)}\right]^{1/2} \ , \quad \text{(A4b)}$$

$$z=\left[\frac{1}{1+\tan^2(\alpha_A)+\tan^2(\alpha_B)}\right]^{1/2}[\tan(\alpha_B)] \ , \quad \text{(A4c)}$$

Note that the signs of the radical terms are a matter of convention. Once this is done for each of the side arms, $\vec{P}$ and $\vec{S}$ will be of the form

$$\vec{P},\vec{S}=x\hat{i}+y\hat{j}+z\hat{k} \ . \quad \text{(A5)}$$

These vectors are then used in Eq. (A1) to determine the orientation angle of the dendrite.

[1] M. E. Glicksman and S. P. March, in *Handbook of Crystal Growth,* edited by D. J. T. Hurle (Elsevier Science Publishers, Amsterdam, 1993), Vol. 1, Pt. b, p. 1081.

[2] G. P. Ivantsov, Dokl. Akad. Nauk SSSR **58**, 56 (1947).

[3] S. C. Huang and M. E. Glicksman, Acta Metall. **29**, 701 (1981).

[4] A. Dougherty and J. P. Gollub, Phys. Rev. A **38**, 3043 (1988).

[5] M. E. Glicksman, M. B. Koss, and E. A. Winsa, Phys. Rev. Lett. **73**, 573 (1994).

[6] J. Maurer, B. Perrin, and P. Tabeling, Europhys. Lett. **14**, 575 (1991).

[7] M. E. Glicksman, M. B. Koss, V. E. Fradkov, M. E. Rettenmayer, and S. S. Mani, J. Cryst. Growth **137**, 1 (1994).

[8] H. Rutten and M. van Venrooij, *Telescope Optics Evaluation and Design* (Willmann-Bell, Inc., Richmond, VA, 1988), p. 206.

[9] D. Kessler and H. Levine, Phys. Rev. A **36**, 4123 (1987).

[10] D. Kessler and H. Levine, Acta Metall. **36**, 2693 (1988).

[11] M. Ben Amar and E. Brener, Phys. Rev. Lett. **71**, 589 (1993).

[12] E. Brener, Phys. Rev. Lett. **71**, 3653 (1993).

[13] E. R. Rubenstein, S. H. Tirmizi, and M. E. Glicksman, J. Cryst. Growth **106**, 89 (1990).

[14] E. Hürlimann, R. Trittibach, U. Bisang, and J. H. Bilgram, Phys. Rev. A **46**, 6579 (1992).

[15] R. Kobayashi, Experimental Mathematics **3**, 59 (1994).

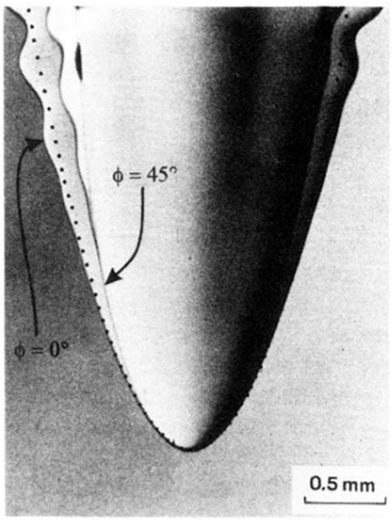

FIG. 1. SCN dendrite tip viewed from two orientations. This illustrates [3] the difference in shape of two superimposed views of the same dendrite. The view from $\phi = 0°$ was made by imaging a dendrite from the direction of the side branches, while $\phi = 45°$ represents a view from between the side branches. A best-fit parabola is indicated by the dotted line between these two profiles.

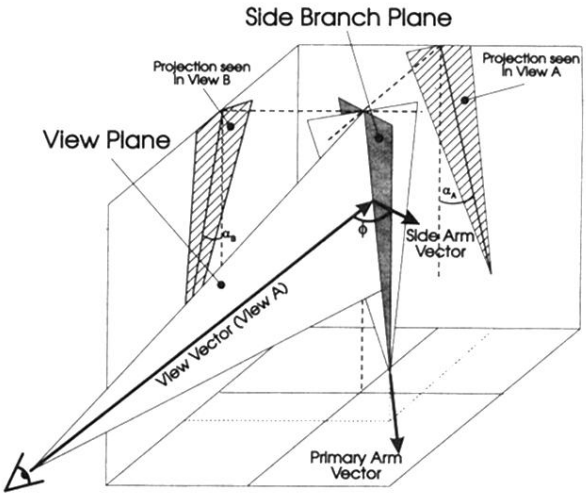

FIG. 12. Schematic representation of dendrite with the projections that would be seen when viewed from two orthogonal directions.

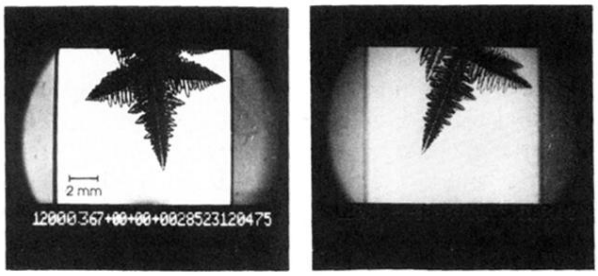

FIG. 5. 35-mm film image of SCN dendrite growing isothermally at $\Delta T = 0.46$ K. Photos are taken along perpendicular axes to produce velocity, size, and shape information.